CERN - EUROPEAN ORGANIZATION FOR NUCLEAR RESEARCH

Submitted to
Nuclear Physics B

CERN/EP/PHYS 76-12
21 April 1976

CHARM SEARCH IN 19 GeV/c π^-p EXCLUSIVE REACTIONS

The Omega Groups(*)

ABSTRACT

A search for charmed particles produced in π^-p exclusive reactions at 19 GeV/c incident beam momentum has been carried out with the Omega spectrometer at CERN. Three million interactions were recorded with a trigger which required a forward K^- or $\bar{p}$ with transverse momentum greater than 0.5 GeV/c. An additional two million triggers were recorded with a forward K^+ or proton, with no transverse momentum restriction. Analysis of the four-constraint final states $K^+K^-\pi^-p$ and $K^+K^-\pi^+\pi^-\pi^-p$ shows no evidence for the associated production of charmed particles. The upper limits for the product of production cross sections and the two charmed particle decay branching ratios are below 100 nb for most of the channels. The experiment was sensitive over a wide range of production angles.

(*) See following page.

PW/mk

B. GHIDINI and F. NAVACH
Università and INFN, Bari.

J. DOWELL, I. KENYON and P. WOODWORTH
Department of Physics, University of Birmingham.

K. MULLER
Physikalisches Institut der Universität, Bonn.

I. SMITH
Daresbury Physics Laboratory, Daresbury.

R. HARTUNG
Universität Freiburg, (Germany).

C. BIZEAU, F. BOURGEOIS, H. DAVIES, J-P. DUFEY, J. EADES, B. FRENCH,
O. GILDEMEISTER, J-C.LASSALLE, S. LAUPER, R. MESSERLI, W. MITAROFF,
C. PALAZZI-CERRINA, L. PAPE, P. SONDEREGGER, R. STRUB, A. THOMPSON,
D. TOWNSEND, D. TREILLE and J. WILSON.
CERN, European Organization for Nuclear Research, Geneva.

T. ARMSTRONG, R. KUMAR and J. SLEEMAN
University of Glasgow, Glasgow.

J.K. BIENLEIN
Deutsches Elektronen-Synchrotron, Hamburg.

M. HOULDEN
University of Liverpool, Liverpool.

L. MANDELLI
Istituto di Fisica dell'Università, Milano and INFN, Milano.

B. BOUQUET, J.M. CHOUNET, A. FERRER, A. LAHELLEC, P. PETROFF, P. ROUDEAU,
J. SIX and H. YOSHIDA
Laboratoire de l'Accélérateur Linéaire, Orsay.

G. De ROSNY, B. DREVILLON, G. IRWIN, A. ROUGE, M. RUMPF, R. SALMERON and
J.P. WUTHRICK
Laboratoire de Physique Nucléaire des Hautes Energies, Ecole Polytechnique,
Palaiseau.

M. CRIBIER, B. GANDOIS, J.R. HUBBARD(*) and A. SAVOY-NAVARRO
Centre d'Etudes Nucléaires, Saclay.

B. AEBISCHER, L. FLURI and K. FREUDENREICH
Laboratorium für Hochenergiephysik, ETH, Zürich.

(*) Correspondence should be addressed to J.R. HUBBARD
D.Ph.P.E. CEN, Saclay, Gif-sur-Yvette, France 91190.

1. INTRODUCTION

An experiment to look for charmed particles produced in $\pi^- p$ interactions at 19 GeV/c has been carried out using the CERN Omega spectrometer. The charm hypothesis holds that charm, like strangeness, should be conserved in strong interactions, so that charmed particles should be produced in pairs. The lowest-mass states are expected to decay mainly through a strangeness-changing weak interaction [1]. Consequently, exclusive reactions have been studied for evidence of associated production of charmed particles, with non-leptonic weak decays into final states containing charged kaons.

The following reactions have been considered:

$$\pi^- p \to D^- D^o p \tag{1}$$
$$\pi^- p \to \bar{D}^o D^o \pi^- p \tag{2}$$
$$\pi^- p \to D^- C^+ \tag{3}$$
$$\pi^- p \to \bar{D}^o C^o \tag{4}$$
$$\pi^- p \to D^- C^o \pi^+ \tag{5}$$
$$\pi^- p \to \bar{D}^o C^+ \pi^- \tag{6}$$
$$\pi^- p \to \bar{D}^o C^o \pi^+ \pi^- \tag{7}$$

with the following decays of the charmed mesons (D) and baryons (C):

$$\begin{aligned} D^o &\to K^- \pi^+ \\ \bar{D}^o &\to K^+ \pi^- \\ &\to K^+ \pi^+ \pi^- \pi^- \\ D^- &\to K^+ \pi^- \pi^- \\ C^o &\to K^- p \\ &\to K^- p \pi^+ \pi^- \\ C^+ &\to K^- p \pi^+ \end{aligned} \tag{8}$$

The expected lifetimes of these weak decays are sufficiently short (10^{-13} to 10^{-11} sec) [1] that the decay tracks would appear to come from the primary vertex. Charmed particles would then appear as narrow peaks on mass plots for reactions such as:

$$\pi^- p \to K^+ K^- \pi^- p \tag{9}$$
$$\pi^- p \to K^+ K^- \pi^+ \pi^- \pi^- p \tag{10}$$

Two samples of data were taken with triggers that required a forward K^- in one case, and a forward K^+ in the other. Together, these data cover the full range of possible production distributions. In the first run (March 1975) three million interactions were recorded with a forward K^- (or $\bar{p}$) with the horizontal component of the transverse momentum greater than 0.5 GeV/c. During the second run (June 1975) an additional two million interactions were recorded with a forward K^+ (or proton), but no restriction on transverse momentum.

Upper limits are presented for charm production in reactions (1) to (7), based on kinematic analysis of the six-prong final state of reaction (10). A further limit for reaction (4) is obtained from the four-prong final state of reaction (9). The data from the two runs were analyzed separately. The K^- run yielded 2996 events with kinematic fits to reaction (9) and 2212 events with fits to reaction (10). The K^+ run yielded 870 events for reaction (9) and 3257 events for reaction (10). The charm search consisted of looking for narrow peaks on the two-dimensional invariant-mass plots corresponding to the hadronic decay modes (8) of possible associated pairs of charmed particles.

2. APPARATUS

The Omega spectrometer [2] is a multi-particle detector at the CERN PS. The 1.8 T superconducting magnet has a useful volume 3 m in diameter by 1.5 m high. Optical spark chambers are arranged about a liquid hydrogen target inside the magnet. These chambers are viewed by television cameras of the plumbicon type [3], producing spark images which are digitized and recorded on-line onto magnetic tape. Multiwire proportional chambers downstream from the target allow selection on multiplicities and momenta. Farther downstream, two multi-cell Cerenkov counters help identify secondary particles above 3 GeV/c.

The experimental set-up for the present experiment is shown in fig. 1. A 60 cm long liquid hydrogen target was surrounded by an 11 cm diameter

cylindrical scintillation counter. The main detector consists of eight forward spark chamber modules nearly perpendicular to the incident beam, with ten spark gaps per module, and four modules parallel to the beam on each side of the target, with eight spark gaps per module. Each forward module has a useful area 126 cm in height by 150 cm in width, and 1.0 cm gaps; the side modules measure 90 cm by 55 cm with 1.2 cm gaps. The spark chamber modules are tilted slightly so as to point toward the cameras, which are 5.5 m above the beam. The stereo angle is 15^{o} for the forward chambers and 12.5^{o} for the side chambers. The demagnification is 1/90. Spark images are digitized with a least count of 0.18 mm in space. The measurement accuracy is $\pm$ 0.5 $(1 + \tan^2 \phi)$ mm, where ϕ is the angle between the track and the normal to the spark chamber plane. Neighbouring sparks are resolved if their separation is greater than about one centimeter.

The first downstream Cerenkov counter was equipped with front and back scintillator hodoscopes and filled with isobutane at atmospheric pressure, to discriminate pions from kaons and protons between 3 and 10 GeV/c. The second Cerenkov counter was filled with freon 13 at 5.5 atmospheres absolute pressure and allowed tagging of kaons and protons between 5 and 10 GeV/c. This counter has a smaller acceptance than the first Cerenkov counter, and was used only to check the reliability of the analysis.

Three sets of multiwire proportional chambers (MWPC) were used for the trigger. Forward multiplicities were selected by a special electronic read-out of MWPC II, which counts clusters of hits in the horizontal and vertical wires. Constraints on the longitudinal and horizontal momentum components of the forward triggering track were imposed by a hardware logic which correlated hits in vertical wires in MWPC's III and IV.

The 19 GeV/c unseparated beam was defined by a set of scintillation counters. Three Cerenkov counters identified the beam particles, and five MWPC's and a scintillator momentum hodoscope measured their momenta and positions. The momentum acceptance was $\pm$ 0.7%, and the momentum accuracy of an individual beam track was $\pm$ 0.3%. The average flux was 1.5×10^5 particles per 350 msec burst, repeated every 2.8 sec.

All data for the events selected were recorded directly onto magnetic tape by means of an on-line data-acquisition system. The dead-time of the system was 18 msec per event, mostly due to the read-out time of the plumbicon cameras.

3. TRIGGERS

The K^- trigger was designed especially to look for the six-prong final state arising from reaction (1),

$$\pi^- p \rightarrow D^- D^o p$$
$$D^o \rightarrow K^- \pi^+$$
$$D^- \rightarrow K^+ \pi^- \pi^-$$

by requiring: a) a hit in the scintillation counter surrounding the target, b) at least three tracks in MWPC II, located 1.1 m downstream from the end of the target, c) a coincidence between MWPC III and MWPC IV to select a forward negative particle with momentum between 3 and 10 GeV/c and with the horizontal component of the transverse momentum greater than 0.5 GeV/c (see fig. 2), and d) a scintillator hodoscope coincidence H1 · H2 with a Cerenkov anti-coincidence to guarantee that this negative trigger particle was heavier than a π^-. During 15 days of production run, 3.2 million events were recorded, 40% of which came from valid interactions in the target. The effective flux was equivalent to 28 events/nb.

The K^+ trigger was designed to look for the associated production of charmed mesons and baryons, with the meson emitted in the forward direction in the c.m. system. Possible three or four-body decays would produce forward K^+ mesons with less tranverse momentum on the average than in the two-body decays. The K^+ trigger was similar to the K^- trigger, but there was no restriction on the K^+ transverse momentum. The Omega magnetic field was reversed in order to bend the triggering track in the same direction in both runs. MWPC II was moved 30 cm closer to the target, and at least four forward tracks were required. Furthermore, several

elements of the back hodoscope (H4) were in anticoincidence to veto diffractive processes giving very fast negative tracks. In a 7 day run, 2.2 million events were recorded, 60% of which were valid triggers. The effective flux was 5 events/nb.

4. ACCEPTANCE AND SENSITIVITY

The acceptance of these triggers was calculated for each reaction using Monte-Carlo techniques. Events were generated with uniform phase-space distributions for the production and for the decays. For example, in reaction (1), with M_D = 2.0 GeV, 20% of the K^- from the decays $D^o \to K^-\pi^+$ go through the atmospheric-pressure Cerenkov counter without giving light, and 40% of them satisfy the transverse momentum criteria of the K^- run. Nearly all the potential triggers satisfy the multiplicity requirement in MWPC II, but 25% of them are lost because of K^- decays, extra particles giving light in the Cerenkov counter, or confusion in the correlation between MWPC III and IV. In 60% of the remaining events all six tracks have projected lengths greater than 25 cm in the optical chambers and momenta greater than 300 MeV/c; only these events are included in the present analysis. The final acceptance is thus 3.6% for the K^- run. For the K^+ run, there is no tranverse momentum restriction, and either the K^+ or the proton in the final state can satisfy the trigger conditions; the total acceptance is 13%.

The sensitivity is the effective flux multiplied by the product of the acceptance and the program efficiency (40% for the six-prong events - see sect. 5). The average sensitivity for phase-space distributed events is therefore .036 x .40 x 28 ev/nb = 0.4 ev/nb for the K^- run, and .13 x .40 x 5 ev/nb = 0.26 ev/nb for the K^+ run.

Sensitivities were also calculated for peripheral production. Events were generated with an exp (2t) dependence, where t is the invariant momentum transfer squared from the incident π^- to the forward charmed particle. For reactions (1) and (2) the meson pair was given an exponential

dependence; in this case, the K^- run was more sensitive than the K^+ run. For the associated-production reactions (3)-(7), the K^- trigger was usually more sensitive for forward baryons, and the K^+ trigger for forward mesons. This difference is illustrated by fig. 3, where the angular dependence of the acceptance for reaction (3), $\pi^- p \to D^- C^+$, is shown for the two runs. The sensitivity is given by the right-hand scale. The contributions of the K^+ and proton triggers in the K^+ run are shown separately by broken lines. The lower acceptance for very forward charmed mesons or baryons is due in large part to the reduced visibility of the associated slow particles. This effect produces a sharp drop in the sensitivity for peripheral production in reaction (4) when the backward meson or baryon has low mass and a four-body decay.

5. DATA ANALYSIS

All events recorded were processed through the Omega pattern-recognition and geometry program ROMEO [4]. This program uses the spark digitizations to find tracks, fit their parameters, and extrapolate them back to locate interaction and decay vertices. In the present analysis, events were accepted only if all tracks had projected lengths greater than 25 cm in the optical spark chambers and momenta greater than 300 MeV/c. Program performance was evaluated by scanning a sample of events. The efficiency for finding and correctly reconstructing the tracks and their interaction vertex was 60% for the four-prong events satisfying the above criteria, and 40% for the six-prong events.

Kinematic fitting was performed only for hypotheses with no missing neutrals. Four-constraint candidates were required to have missing transverse momentum (P_T) less than 150 MeV/c and missing longitudinal momentum ($|P_L|$) less than 500 MeV/c. The missing P_L for four-prong events from the K^- run is shown in fig. 4. The events with small missing P_T (cross-hatched in the figure) form a peak at zero with a width of 320 MeV/c (FWHM). We estimate that less than 5% of the good candidates are eliminated by our missing momentum selections.

In order to demonstrate the separation of the K^+K^- and $p\bar{p}$ hypotheses for these data, we have calculated the mass of the $X^{\pm}$ particles for the reactions $\pi^- p \to X^+X^-\pi^- p$ and $\pi^- p \to X^+X^-\pi^+\pi^-\pi^- p$, where the triggering track is taken to be an X^- for the K^- run or an X^+ for the K^+ run [5]. In fig. 5a the $X^{\pm}$ mass is shown for the four-prong events from the K^- run, with the X^+ taken as the fastest of the two positive tracks. The peaks at the kaon and proton masses are clearly separated. A small peak at the pion mass is due to π^- which interact before the Cerenkov counter, producing slower tracks which satisfy the trigger conditions. The six-prong events are shown in fig. 5(b), with the X^+ taken as the fastest of the three positive tracks. Most of the K^+K^- signal is contained in these clearly-defined peaks; but all mass permutations are interesting for the charm search, so appreciable ambiguities remain.

The program KOMEGA, running under the HYDRA system [6], was used for the kinematic analysis. Fits with a chi-squared probability less than 1% or less than one-tenth that of the best fit were rejected. The results are presented in table I. Some events in the K^+ run are identified as multi-pion production, with the proton in the final state satisfying the trigger conditions.

6. CHARM SEARCH

We have searched for charm production in the exclusive reactions (1)-(7) with charmed particle decays leading to the four-prong and six-prong final states of reactions (9) and (10). Only reaction (4) has possible charm decays which could contribute to the four-prong final state. It has in addition, two sets of decay modes which would give six-prong final states. Each of the other reactions has a unique set of charm decays leading to the six-prong final state.

For each reaction the effective mass of the decay products of one charmed meson or baryon was plotted against the effective mass of the associated charmed meson. We then looked for narrow peaks on these two-

dimensional mass plots corresponding to weak decays of the lowest-mass charmed mesons and baryons. The search was limited to charmed meson masses above 1.5 GeV and charmed baryons above 2.0 GeV. Typical mass plots are shown in figs 6-10(a) for the K^- run and 6-10(b) for the K^+ run.

The meson-pair reactions (1) and (2) are shown in figs 6 and 7. The two weakly-decaying mesons should have the same mass, except for a small electromagnetic mass difference between the D^- and the D^o. For the D^-D^op final state, the mass of the exotic combination $K^+\pi^-\pi^-$ ($I_z = -3/2$) would then be about equal to that of the non-exotic combination $K^-\pi^+$. The mass distributions along the diagonals are shown separately on figs 6 and 7. Double $K^*(890)$ production is evident in fig. 7, but no significant peaks are seen above 1.5 GeV, either on the diagonal or in the surrounding region.

Examples of mass plots for charmed meson-baryon associated production are shown in figs 8-10. We consider only charmed baryons which are lighter than the sum of the charmed meson mass and the nucleon mass ($M_C \lesssim M_D + M_N$); otherwise, the baryon would decay strongly into the meson and the nucleon, and we could observe them in the meson-pair reactions shown above. Figs 8 and 9 represent two more interpretations of the six-prong data, corresponding to the two-body production modes (3) and (4). These spectra are quite different for the K^- and K^+ runs, due to the different trigger conditions. Fig. 10 shows the four-prong mass plots corresponding to reaction (4). Both the $K^*(890)$ and the $K^*(1420)$ are visible in these final states. But no strong narrow peaks are evident in the regions of interest on any of the mass plots studied.

A systematic search of all relevant mass plots was carried out with a computer program. An integrated probability was calculated for each bin by summing the Poisson distribution (with a mean equal to the background for that bin) over population values equal to and greater than the population observed. The background was taken as the average population of the 25 nearest bins, including the bin of interest. The fitted resolution for the various masses was 25-30 MeV (FWHM), so we have looked for a

narrow peak in any 50 MeV by 50 MeV bin. The search was repeated with the bins displaced successively by a half bin. Bins which had low probabilities were studied in more detail. In particular, if the probability for a bin was small on one mass plot, we looked for any accumulation of events near the same mass values on the other mass plots for each of the two runs. No persistent signals were seen.

We have investigated the validity of these Poisson probability calculations for our data. Simple Poisson fluctuations of the bin populations would result in a flat frequency distribution for the integrated probabilities, if the background estimations are adequate. The experimental distribution, shown in log-log form in fig. 11, follows the ideal distribution rather well. The smallest probability observed in any region of interest to the charm search was 10^{-3}. This can be compared with the probability of 10^{-13} calculated for the double $K^*(890)$ on fig. 7. The bin with the probability of 10^{-3} is compatible with the rest of the frequency distribution, whereas the double K^* is not. We conclude that there is no evidence for associated production of charmed particles in these data.

Upper limits at the 95% confidence level were calculated for charm production in reactions (1) to (7). Each mass plot was scanned to find the bin having the largest possible signal above background, allowing for Poisson variations of the bin population. Here the background was taken as the average population of the 24 nearest bins, excluding the bin of interest. The signal upper limits were corrected for events which would have fallen outside the bin due to the experimental mass resolution.

Cross section upper limits were found for each reaction by dividing the signal upper limits by the sensitivity. Results are presented in table II for phase space angular distributions and for peripheral production. These are 95% confidence level upper limits for the product of the cross section and the two charmed-particle decay branching ratios. For each entry, the upper limit is given for the run which was most sensitive to the channel and production mode considered.

7. CONCLUSIONS

We have searched for associated production of charmed particles in exclusive reactions with visible non-leptonic weak decays into four-constraint final states. The total c.m. energy available was 6.0 GeV. The sensitivity of the experiment was about 0.4 ev/nb. We looked for mesons with masses above 1.5 GeV and baryons above 2.0 GeV. The experiment was sensitive over the full range of possible production distributions. No evidence for charm production was seen. The upper limits (95% confidence level) for the cross sections multiplied by the product of the two decay branching ratios are between 40 nb and 2 μb, depending on the channel, the production mode, and the charmed particle masses (see table II).

8. COMPARISON WITH OTHER RESULTS

We can compare our results with the results published by Baltay et al. [7], for exclusive final states in 15 GeV/c $\pi^+ p$ interactions. Their total c.m. energy was 5.4 GeV. They looked at final states containing at least one neutral strange particle (K^o or Λ) and no more than one missing π^o. After summing over several possible charm decay modes, they find limits of 1.5 to 3.7 μb for specific associated production reactions. The present experiment is at least one order of magnitude more sensitive than that of Baltay et al.

Several experiments have looked for charmed particles in inclusive hadronic reactions (one-dimensional mass plots). The most sensitive search was that of Aubert et al. [8], who studied the interactions of 30 GeV/c protons in a beryllium target, using a bi-spectrometer. They report upper limits of a few nb for two-body decays of new particles produced at rest in the proton-nucleon c.m. system. Bläser et al. [9] give upper limits of 50 nb/nucleon for two-body decays of charmed-particles produced by dissociation of neutrons with average momenta of 200 GeV/c. Bubble chamber results are less sensitive. Baltay et al., in the 15 GeV/c $\pi^+ p$ experiment cited above [7], looked for single charmed-particle decays into a Λ or K^o and up to eight charged pions. Ward et al. [10] have looked for similar decay modes with a smaller sample of np interactions at 24 GeV/c. Carlsson et al. [11],

with $\bar{p}p$ interactions at 9.1 GeV/c, looked for charmed meson decays with a sensitivity of only 0.15 events/μb. None of these experiments found narrow peaks which could be evidence for charm production.

Boyarski et al. [12] have looked for non-leptonic decays of charmed particles produced in e^+e^- interactions at SLAC. Again, no peaks were seen. These results can be used to set limits on specific hadronic decays of charmed mesons [13]. On the other hand, some observations which may be interpreted as evidence for charm production have been made in neutrino interactions [14, 15, 16], although no convincing peak has yet been observed on any mass distribution.

ACKNOWLEDGEMENTS

The encouragement of the CERN Electronics Experiments Committee was an important factor in making this experiment possible. Thanks are due to the CERN PS staff and to the Omega technical staff for their dedicated assistance. We would also like to thank the staffs of the computer centers at CERN [CDC 7600], Daresbury [IBM 370/165], and Paris IN2P3 [CDC 6600] for the efficient and rapid processing of our large volume of data. Finally, it is a pleasure to acknowledge many useful discussions with Mary K. Gaillard and John Ellis.

REFERENCES

[1] See M.K. Gaillard, B.W. Lee and J.L. Rosner, Rev. Mod. Phys. 47 (1975) 277.

[2] O. Gildemeister, International Conference on Instrumentation for High Energy Physics, Frascati 1973.

[3] J. Garvey, TV Cameras in High-energy Physics Experiments. Paper submitted to the International Conference on Instrumentation for High Energy Physics, Frascati 1973.

[4] CERN ROMEO Manual.

[5] R. Ehrlich, R.J. Plano and J.B. Whittaker, Phys. Rev. Letters 20 (1968) 686.

[6] CERN HYDRA System Manual.

[7] C. Baltay, C.V. Cautis, D. Cohen, S. Csorna, M. Kalelkar, D. Pisello, E. Schmidt, W.D. Smith and N. Yeh, Phys. Rev. Letters 34 (1975) 1118.

[8] J.J. Aubert, U. Becker, P.J. Biggs, J. Burger, M. Chen, G. Everhart, J. Leong, T.G. Rhoades, M. Rhode, T. Sanford, Samuel C.C. Ting, W.H. Toki, Sau Lan Wu, J.W. Glenn III and Y.Y. Lee, Phys. Rev. Letters 35 (1975) 416.

[9] E.J. Bleser, B. Gobbi, L. Kenah, J. Keren, J. Rosen, R. Ruchti, H. Scott, D. Spelbring, J. Biel, C. Bromberg, T. Ferbel, P. Slattery, D. Underwood and D. Freytag, Phys. Rev. Letters 35 (1975) 76.

[10] D.R. Ward, R.E. Ansorge, J.R. Carter, R.P. Mount, W.W. Neale and J.G. Rushbrooke, Nucl. Phys. B101 (1975) 29.

[11] R. Carlsson, G. Ekspong, S.O. Holmgren, S. Nilsson, R. Stenbacka, Ch. Walck, P. Gregory, P. Mason, H. Muirhead and G. Warren, Nucl. Phys. B99 (1975) 451.

[12] A.M. Boyarski et al., Phys. Rev. Letters 35 (1975) 196.

[13] Martin B. Einhorn and C. Quigg, Phys. Rev. Letters 35 (1975) 1114.

[14] E.G. Cazzoli, A.M. Cnops, P.L. Connolly, R.I. Louttit, M.J. Murtagh, R.B. Palmer, N.P. Samios, T.T. Tso and H.H. Williams, Phys. Rev. Letters 34 (1975) 1125.

[15] H. Deden et al., Phys. Letters 58B (1975) 361;
J. Blietschau et al., Phys. Letters 60B (1976) 207.

[16] J. von Krogh et al., Phys. Rev. Letters 36 (1976) 710.

TABLE CAPTIONS

Table 1 Results of kinematic fitting.
X^+X^- = $\pi^+\pi^-$, K^+K^-, or $p\bar{p}$ for the different hypotheses. The number of events having fits to each hypothesis is given, as well as the total number of K^+K^- fits. The ambiguous events in the $K^+K^-/p\bar{p}$ column are also counted in both the K^+K^- and $p\bar{p}$ columns.

Table 2 Upper limits (95% confidence level) for charm production cross sections times decay branching fraction for $M_D > 1.5$ GeV and $M_C > 2.0$ GeV. Forward mesons and baryons were generated with an exp (2t) dependence for the acceptance calculations. The visibility for four-body decays of backward-produced particles is highly mass-dependent. The following limits apply to more restricted mass regions: (a) 200 nb for $M_c + M_D > 4.0$ GeV for backward-produced mesons; (b) 500 nb for $M_c > 2.3$ GeV and 300 nb for $M_c > 2.5$ GeV for backward-produced baryons.

TABLE I

Reaction	Trigger	Number of events				Number of Fits
		$\pi^+\pi^-$	K^+K^-	$p\bar{p}$	$K^+K^-/p\bar{p}$	K^+K^-
$\pi^- p \to X^+X^-\pi^- p$	$K^-/\bar{p}$	-	2996	4322	17	3301
$\pi^- p \to X^+X^-\pi^- p$	K^+/p	25	870	1111	40	1144
$\pi^- p \to X^+X^-\pi^+\pi^-\pi^- p$	$K^-/\bar{p}$	-	2212	2497	312	2827
$\pi^- p \to X^+X^-\pi^+\pi^-\pi^- p$	K^+/p	376	3257	3356	863	5657

TABLE II

Charm Reaction	Charm Decays	Cross Section Upper Limits (nb)		
		Phase Space	Forward Mesons	Forward Baryons
$\pi^- p \to D^- D^o p$	$D^- \to K^+\pi^-\pi^-$; $D^o \to K^-\pi^+$	75	50	-
$\pi^- p \to \bar{D}^o D^o \pi^- p$	$\bar{D}^o \to K^+\pi^-$; $D^o \to K^-\pi^+$	80	60	-
$\pi^- p \to D^- C^+$	$D^- \to K^+\pi^-\pi^-$; $C^+ \to K^- p\pi^+$	65	80	200
$\pi^- p \to \bar{D}^o C^o$	$\bar{D}^o \to K^+\pi^+\pi^-\pi^-$; $C^o \to K^- p$	75	100	2000 (a)
$\pi^- p \to \bar{D}^o C^o$	$\bar{D}^o \to K^+\pi^-$; $C^o \to K^- p\pi^+\pi^-$	65	1000 (b)	55
$\pi^- p \to \bar{D}^o C^o$	$\bar{D}^o \to K^+\pi^-$; $C^o \to K^- p$	40	200	40
$\pi^- p \to D^- C^o \pi^+$	$D^- \to K^+\pi^-\pi^-$; $C^o \to K^- p$	45	95	60
$\pi^- p \to \bar{D}^o C^+ \pi^-$	$\bar{D}^o \to K^+\pi^-$; $C^+ \to K^- p\pi^+$	55	120	60
$\pi^- p \to \bar{D}^o C^o \pi^+\pi^-$	$\bar{D}^o \to K^+\pi^-$; $C^o \to K^- p$	50	70	40

FIGURE CAPTIONS

Fig. 1 Experimental set-up viewed from above. The limits of the superconducting coils are shown by the two concentric circles. No use was made of the time-of-flight counter (TOF) in the present analysis.

Fig. 2 Horizontal component of the transverse momentum (Py) of the triggering track for a sample of events from the K^- run. The effective Py cut imposed varies from 0.6 GeV/c at the beginning of the target to 0.5 GeV/c at its end.

Fig. 3 Monte-Carlo acceptance and sensitivity for $\pi^- p \to D^- C^+$ as a function of the D^- production cosine in the c.m. system. The scales have been chosen such that the acceptance and the sensitivity for the K^+ run are represented by a single set of curves. The curves were calculated for $M_{D^-} = 2.0$ GeV, $M_{C^+} = 2.75$ GeV.

Fig. 4 Missing longitudinal momentum (P_L) in the laboratory system for a sample of four-prong events from the K^- run. The cross-hatched events have missing transverse momentum (P_t) less than 80 MeV/c; this cut is more restrictive than that used for selecting four-constraint candidates for kinematic fitting.

Fig. 5 Separation of four-constraint hypotheses: (a) for four-prong events and (b) for six-prong events from the K^- run. The square of the mass of the $X^{\pm}$ particle is plotted, where the X^- is the trigger particle, and the X^+ is taken as the fastest of the positive tracks for this figure.

Fig. 6 Search for $\pi^- p \to D^- D^0 p$. Effective mass plot of $K^+\pi^-\pi^-$ vs. $K^-\pi^+$ for $\pi^- p \to K^+K^-\pi^+\pi^-\pi^- p$, at 19 GeV/c. The mass along the diagonal (mass difference less than 35 MeV) is shown in 50 MeV bins.

FIGURE CAPTIONS (Cont'd)

Fig. 7 Search for $\pi^- p \to \bar{D}^o D^o \pi^- p$. Effective mass plot of $K^+\pi^-$ vs. $K^-\pi^+$ for $\pi^- p \to K^+K^-\pi^+\pi^-\pi^- p$ at 19 GeV/c. The mass along the diagonal is shown in 50 MeV bins.

Fig. 8 Search for $\pi^- p \to D^- C^+$. Effective mass plot of $K^+\pi^-\pi^-$ vs. $K^- p\pi^+$ for $\pi^- p \to K^+K^-\pi^+\pi^-\pi^- p$ at 19 GeV/c.

Fig. 9 Search for $\pi^- p \to \bar{D}^o C^o$ in the six-prong events. Effective mass plot of $K^+\pi^+\pi^-\pi^-$ vs $K^- p$ for $\pi^- p \to K^+K^-\pi^+\pi^-\pi^- p$ at 19 GeV/c.

Fig. 10 Search for $\pi^- p \to \bar{D}^o C^o$ in the four-prong events. Effective mass plot of $K^+\pi^-$ vs. $K^- p$ for $\pi^- p \to K^+K^-\pi^- p$ at 19 GeV/c.

Fig. 11 Integrated Poisson probabilities for all bins of interest to the charm search. The mean (μ) was taken equal to the average population in the region of the bin; n_{obs} is the observed bin population. Data from the K^- and K^+ runs were plotted together. The solid curve shows the distribution expected in the absence of narrow peaks.

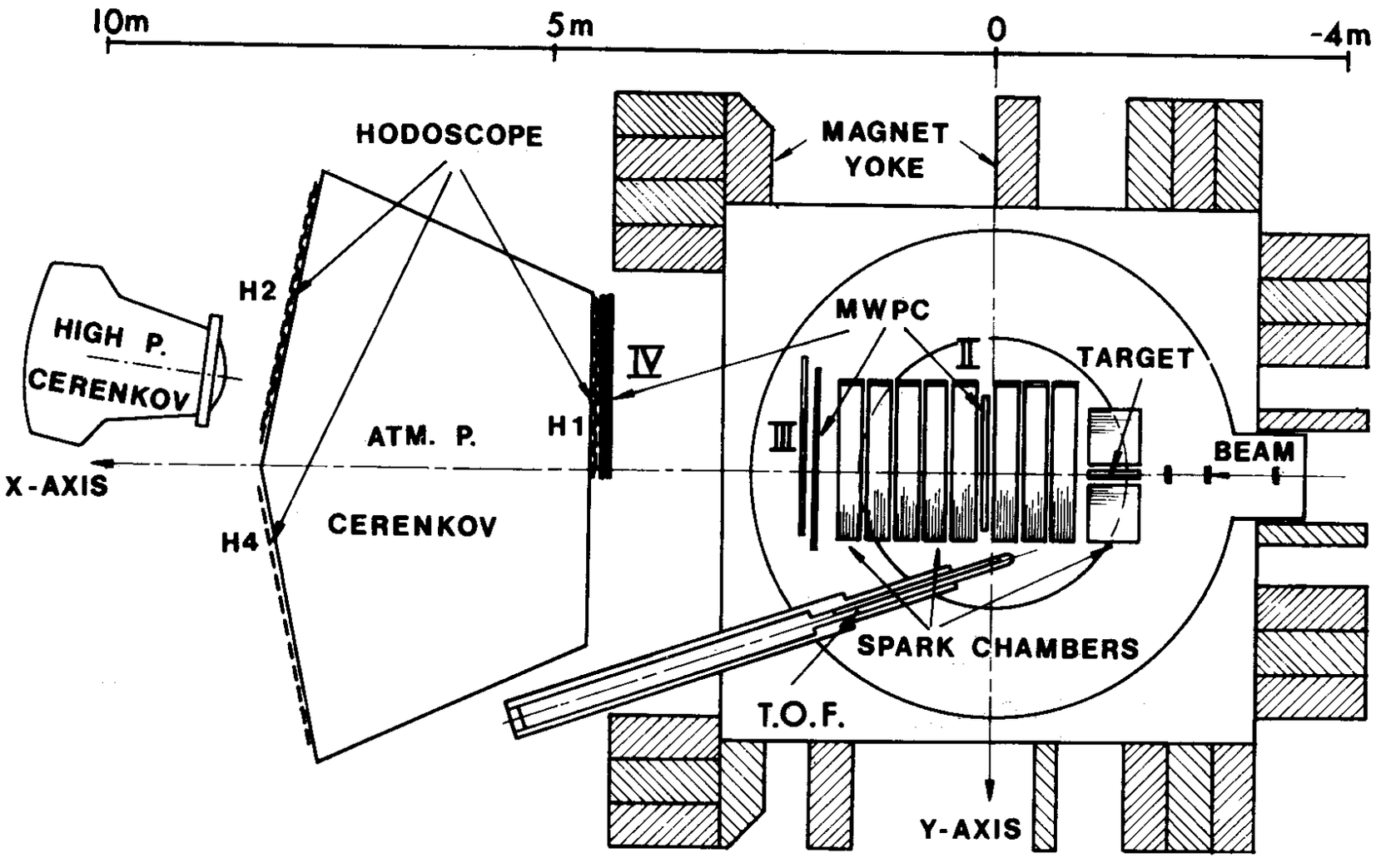
10m
5m
0
-4m
HODOSCOPE
MAGNET
YOKE
H2
HIGH P.
CERENKOV
MWPC
IV
II
TARGET
III
ATM. P.
H1
BEAM
X-AXIS
H4
CERENKOV
SPARK CHAMBERS
T.O.F.
Y-AXIS

fig. I

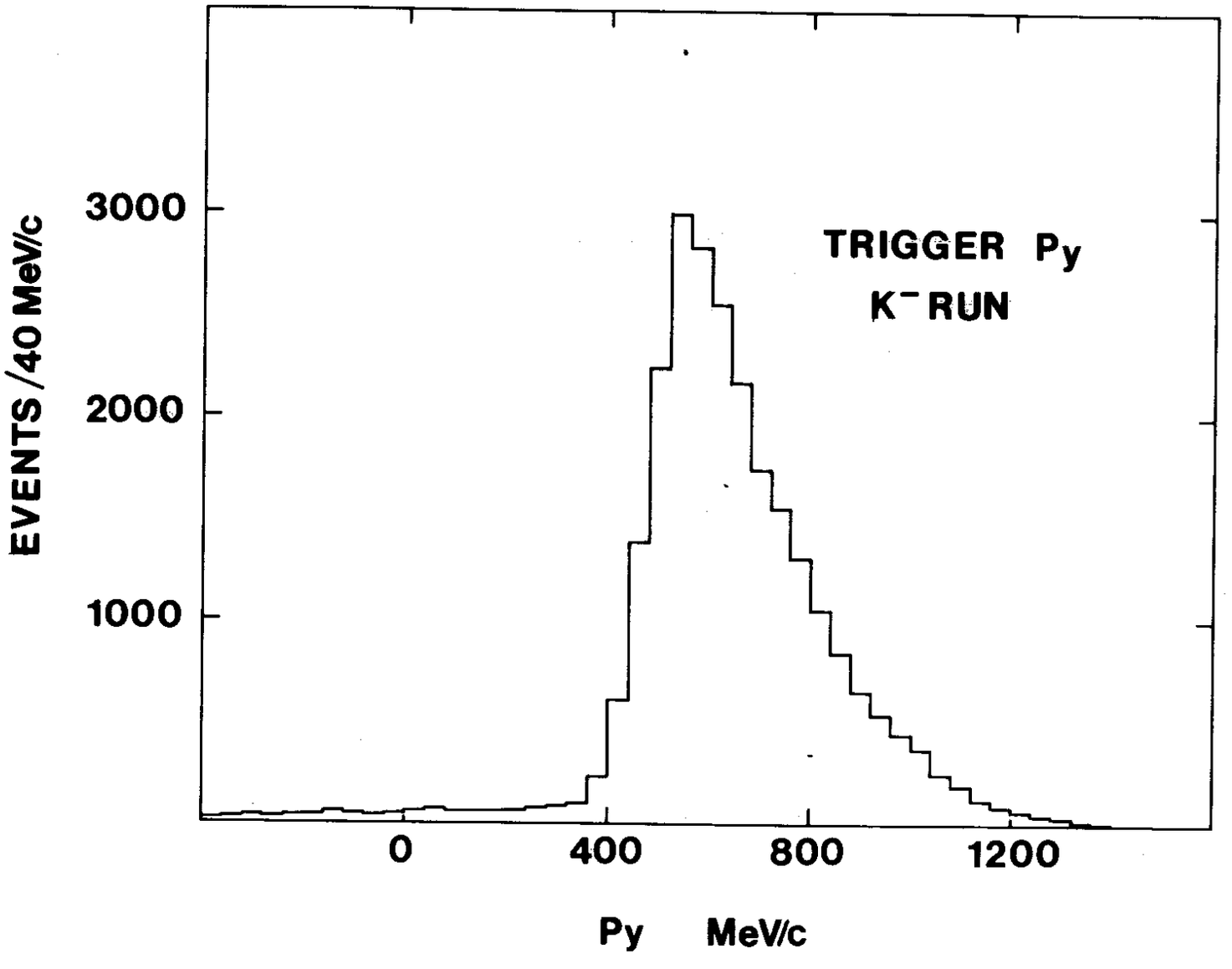
EVENTS /40 MeV/c
3000
2000
1000
TRIGGER Py
K⁻ RUN
0
400
800
1200
Py MeV/c

fig. 2

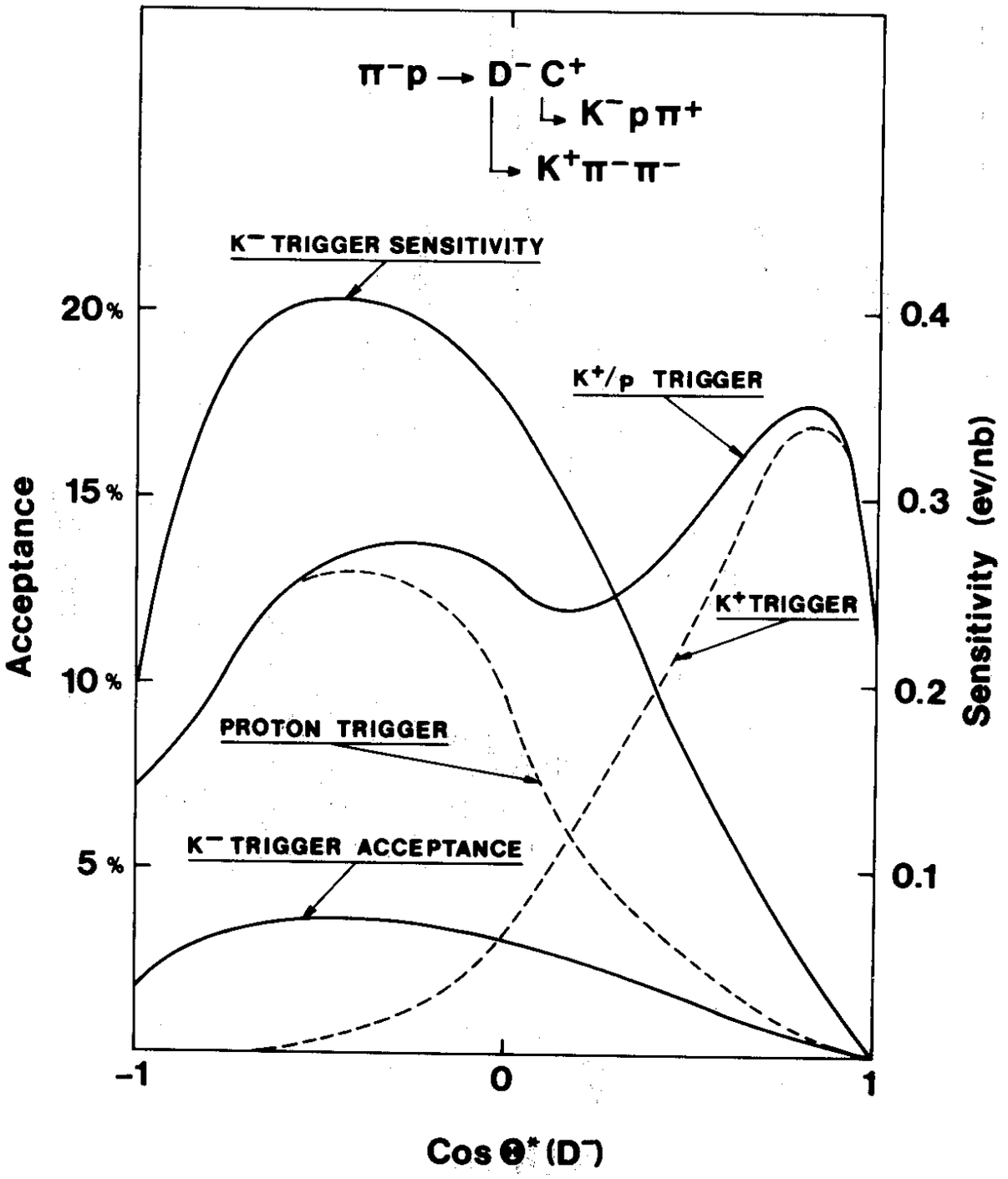
π⁻p → D⁻ C⁺
↳ K⁻pπ⁺
↳ K⁺π⁻π⁻
K⁻ TRIGGER SENSITIVITY
K⁺/p TRIGGER
K⁺ TRIGGER
PROTON TRIGGER
K⁻ TRIGGER ACCEPTANCE
20%
15%
10%
5%
Acceptance
0.4
0.3
0.2
0.1
Sensitivity (ev/nb)
-1
0
1
Cos Θ* (D⁻)

fig. 3

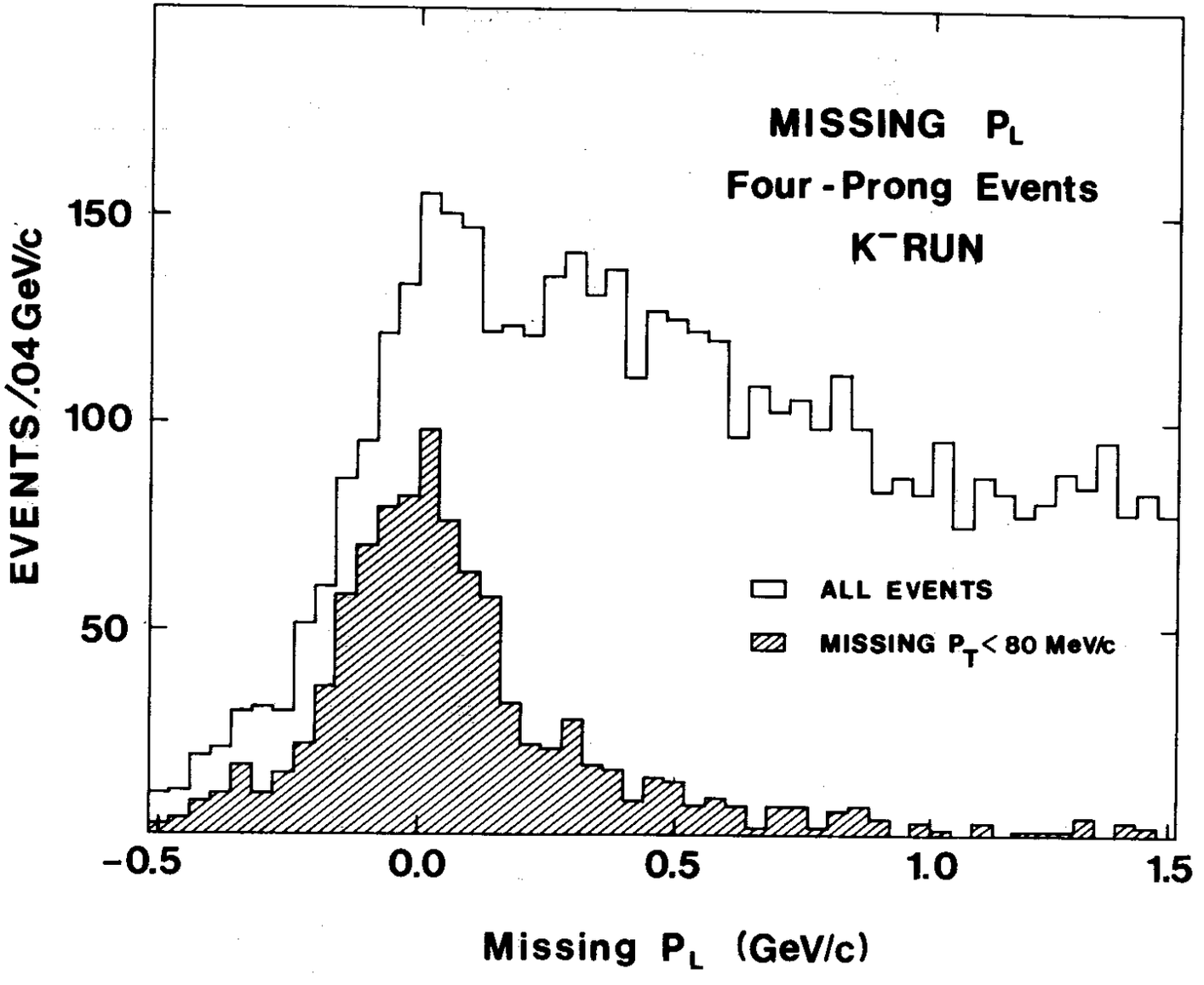
MISSING P_L
Four-Prong Events
K^- RUN
ALL EVENTS
MISSING P_T < 80 MeV/c
EVENTS/.04 GeV/c
150
100
50
-0.5
0.0
0.5
1.0
1.5
Missing P_L (GeV/c)

fig.4

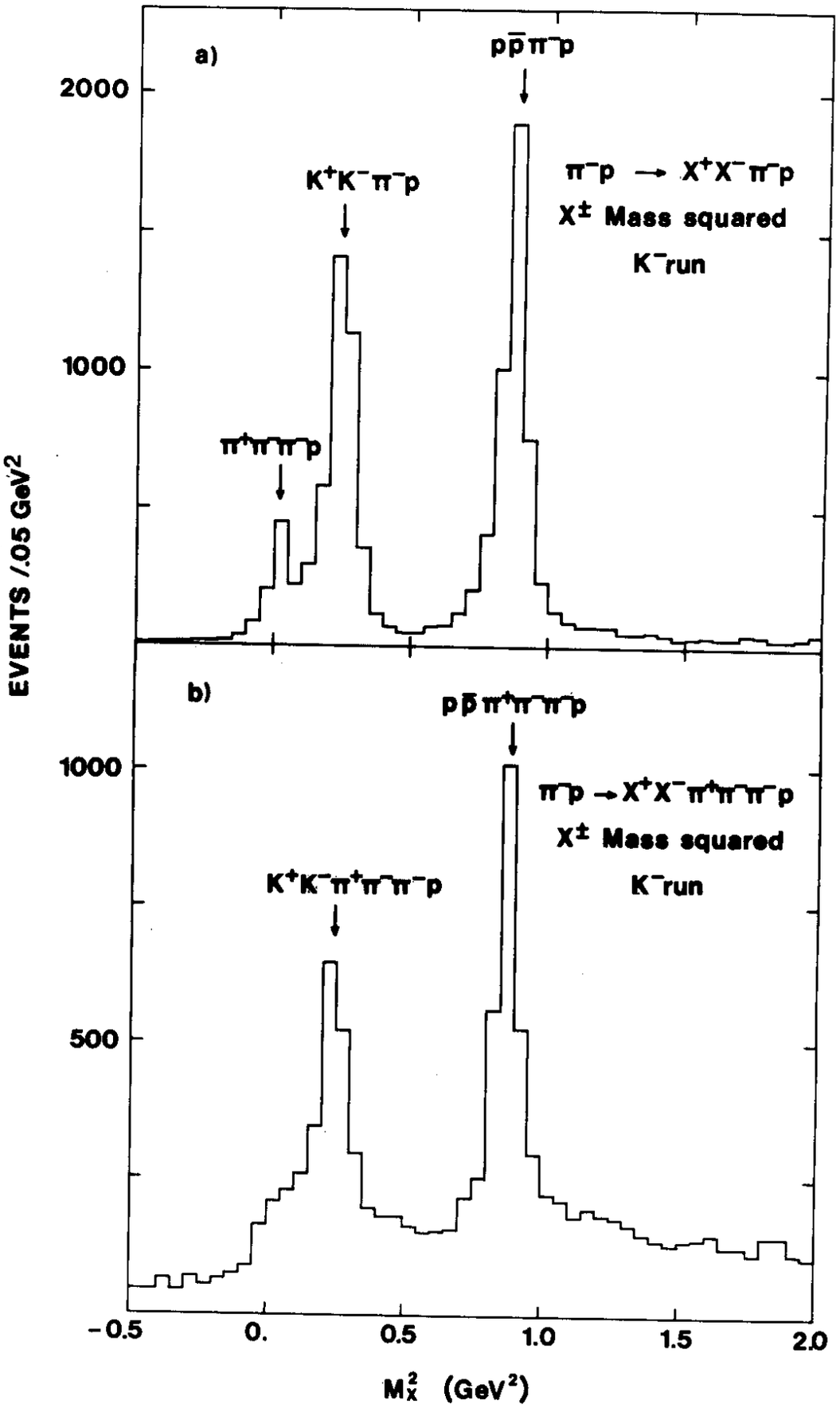
a)
$p\bar{p}\pi^-p$
$K^+K^-\pi^-p$
$\pi^+\pi^-\pi^-p$
$\pi^-p \rightarrow X^+X^-\pi^-p$
$X^\pm$ Mass squared
K^-run
2000
1000
b)
$p\bar{p}\pi^+\pi^-\pi^-p$
$K^+K^-\pi^+\pi^-\pi^-p$
$\pi^-p \rightarrow X^+X^-\pi^+\pi^-\pi^-p$
$X^\pm$ Mass squared
K^-run
1000
500
EVENTS /.05 GeV^2
-0.5
0.
0.5
1.0
1.5
2.0
M_X^2 (GeV^2)

fig. 5

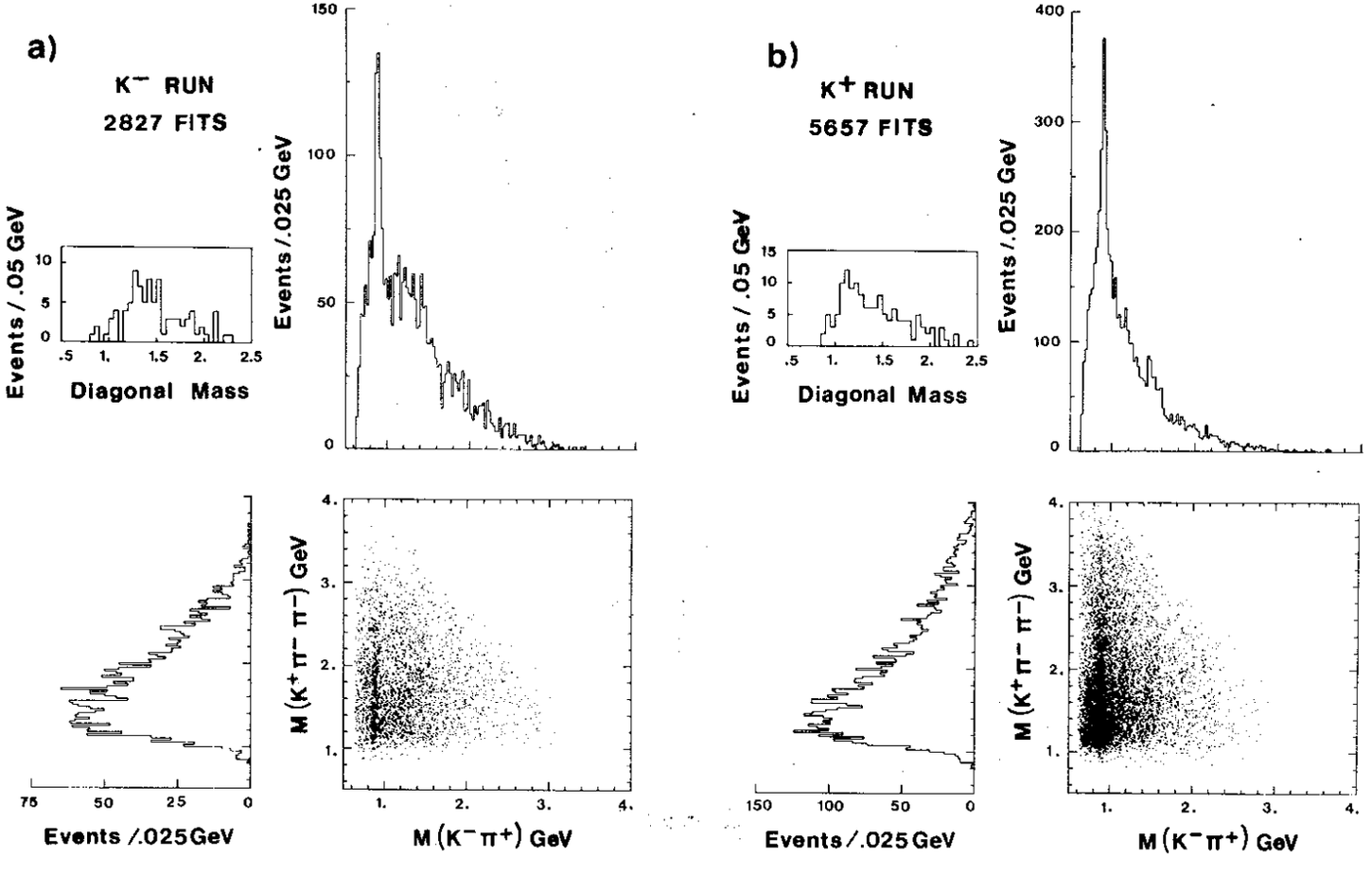
a)
K⁻ RUN
2827 FITS
Events / .05 GeV
Diagonal Mass
Events /.025 GeV
Events /.025 GeV
M (K⁺π⁻ π⁻) GeV
M (K⁻π⁺) GeV
b)
K⁺ RUN
5657 FITS
Events / .05 GeV
Diagonal Mass
Events /.025 GeV
Events /.025 GeV
M (K⁺π⁻ π⁻) GeV
M (K⁻π⁺) GeV

FIG. 6

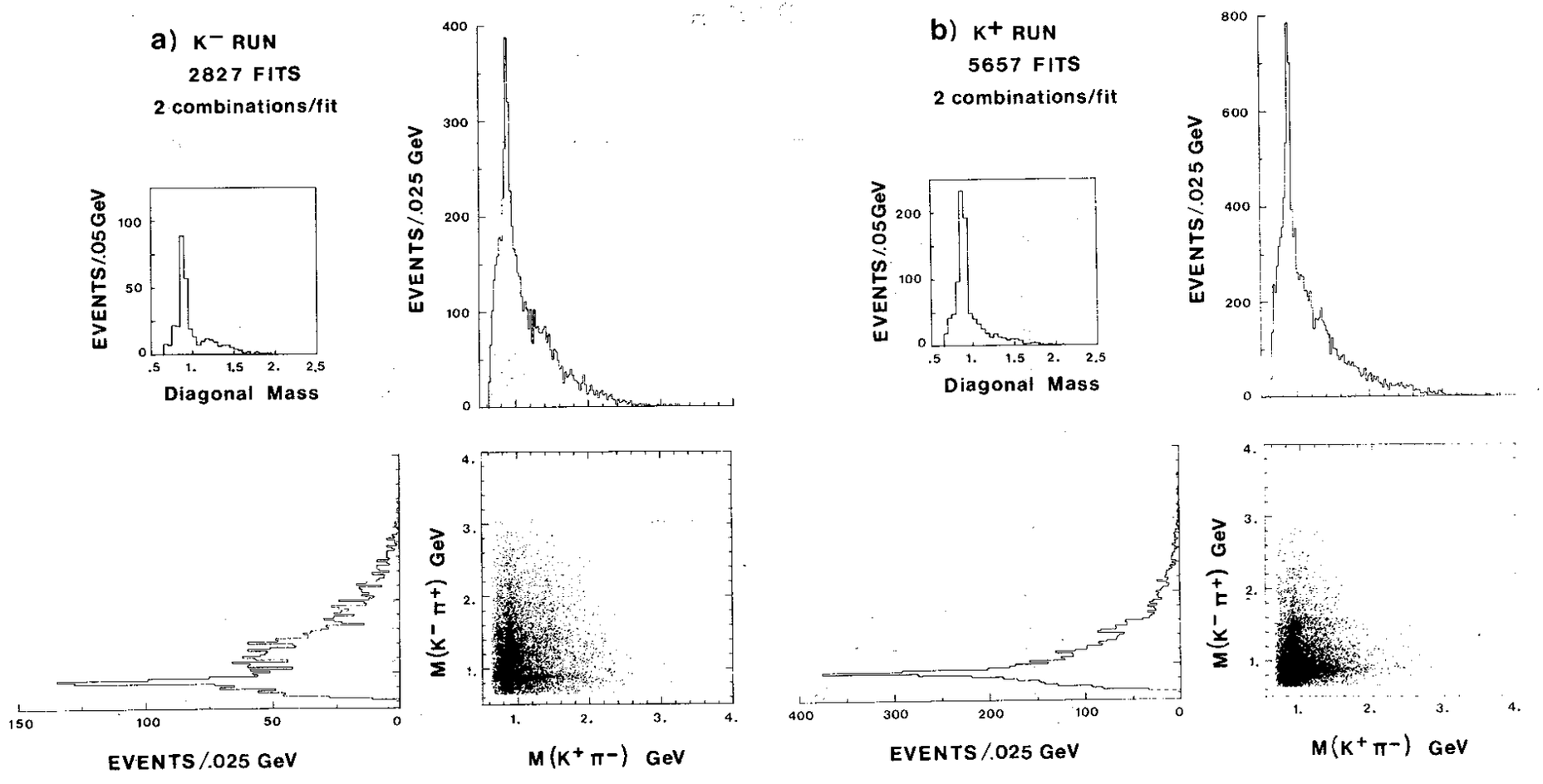
a) K⁻ RUN
2827 FITS
2 combinations/fit
EVENTS/.05GeV
Diagonal Mass
EVENTS/.025 GeV
M(K⁻π⁺) GeV
M(K⁺π⁻) GeV
EVENTS/.025 GeV
b) K⁺ RUN
5657 FITS
2 combinations/fit
EVENTS/.05GeV
Diagonal Mass
EVENTS/.025 GeV
M(K⁻π⁺) GeV
M(K⁺π⁻) GeV
EVENTS/.025 GeV

FIG. 7

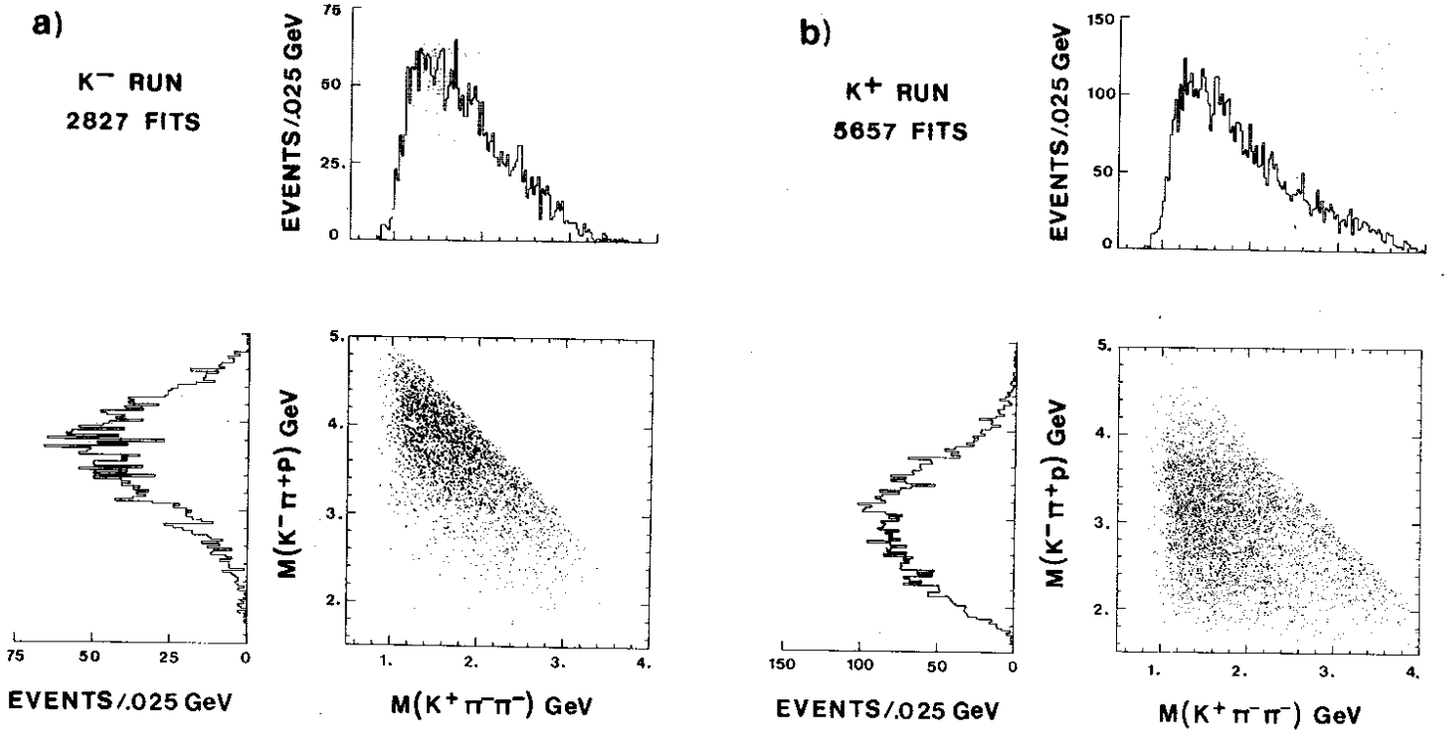
a)
K⁻ RUN
2827 FITS
EVENTS/.025 GeV
M(K⁻π⁺P) GeV
M(K⁺π⁻π⁻) GeV
EVENTS/.025 GeV
b)
K⁺ RUN
5657 FITS
EVENTS/.025 GeV
M(K⁻π⁺p) GeV
M(K⁺π⁻π⁻) GeV
EVENTS/.025 GeV

FIG. 8

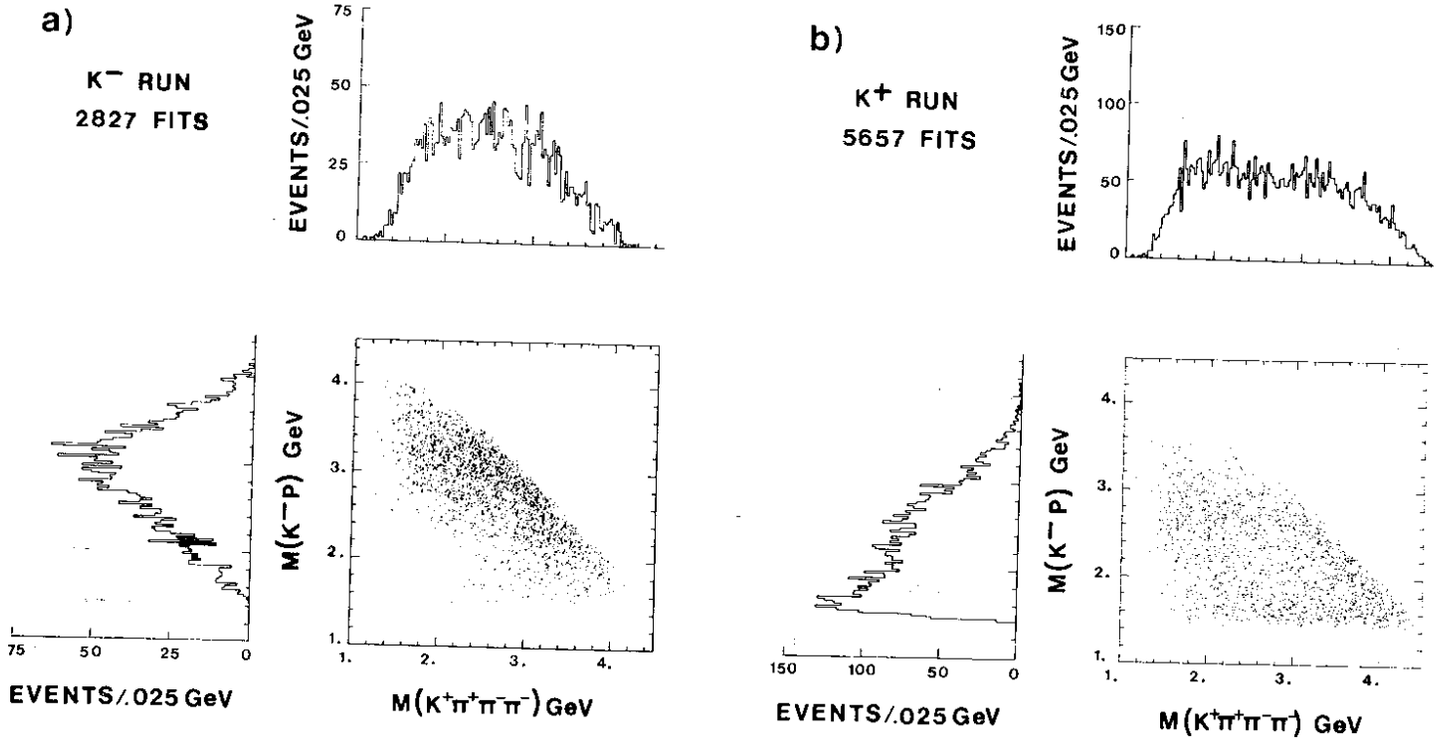
a)
K⁻ RUN
2827 FITS
EVENTS/.025 GeV
75
50
25
0
EVENTS/.025 GeV
M(K⁻P) GeV
M(K⁺π⁺π⁻π⁻) GeV
b)
K⁺ RUN
5657 FITS
EVENTS/.025 GeV
150
100
50
0
EVENTS/.025 GeV
M(K⁻P) GeV
M(K⁺π⁺π⁻π⁻) GeV

FIG. 9

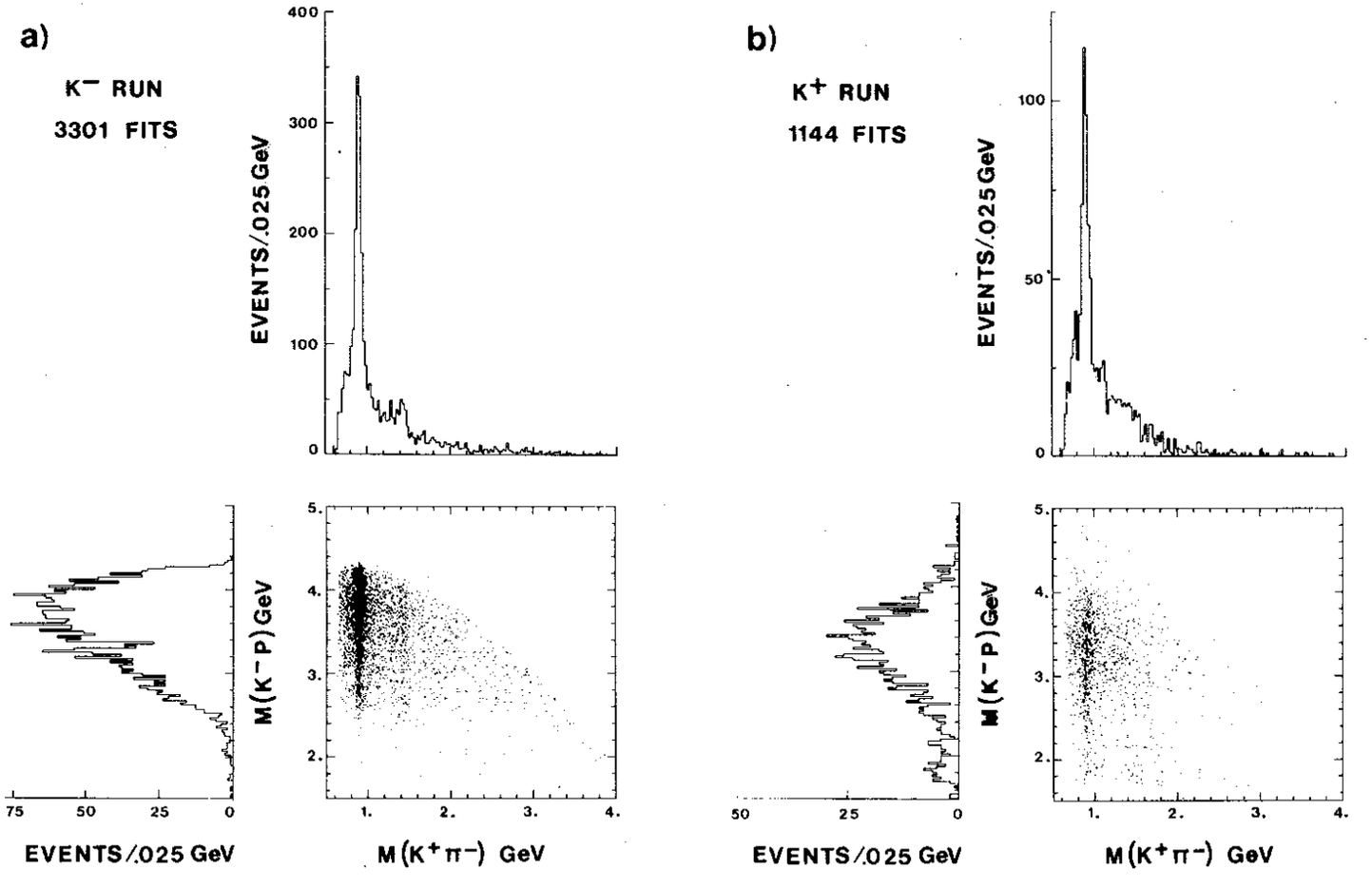
a)
K⁻ RUN
3301 FITS
EVENTS/.025 GeV
M(K⁻P) GeV
M(K⁺π⁻) GeV
b)
K⁺ RUN
1144 FITS
EVENTS/.025 GeV
M(K⁻P) GeV
M(K⁺π⁻) GeV

FIG. 10

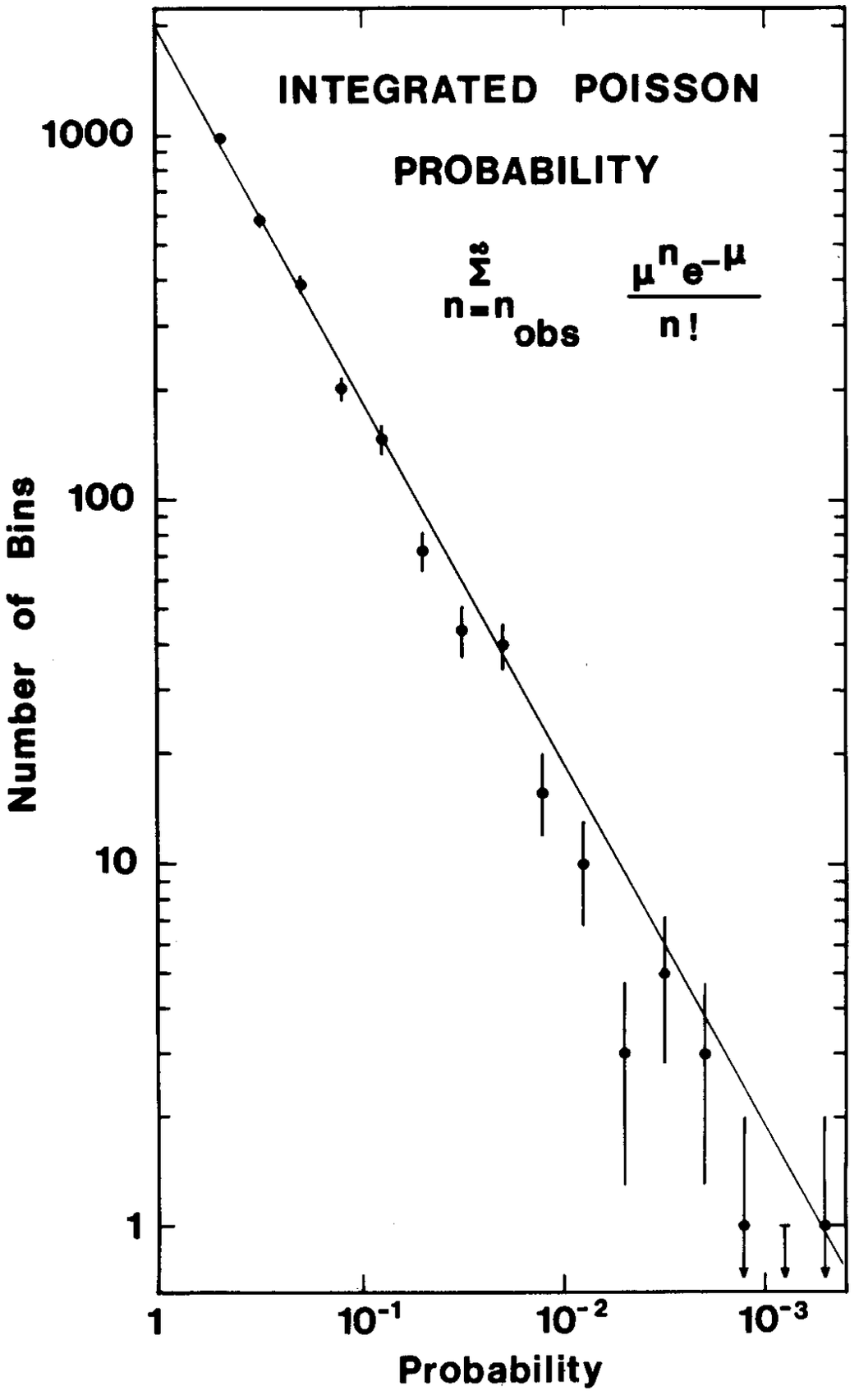
INTEGRATED POISSON
PROBABILITY
$\sum_{n=n_{obs}}^{\infty} \frac{\mu^n e^{-\mu}}{n!}$
1000
100
10
1
Number of Bins
1
10^{-1}
10^{-2}
10^{-3}
Probability

fig. 11